Surface-Step-Induced Oscillatory Oxide Growth

Liang Li,[1] Langli Luo,[1] Jim Ciston,[2,4] Wissam A. Saidi,[3] Eric A. Stach,[4] Judith C. Yang,[5] and Guangwen Zhou[1,*]
[1]Department of Mechanical Engineering and Multidisciplinary Program in Materials Science and Engineering, State University of New York at Binghamton, New York 13902, USA
[2]National Center for Electron Microscopy, Lawrence Berkeley National Laboratory, Berkeley, California 94720, USA
[3]Department of Mechanical Engineering and Materials Science, University of Pittsburgh, Pittsburgh, Pennsylvania 15261, USA
[4]Center for Functional Nanomaterials, Brookhaven National Laboratory, Upton, New York 11973, USA
[5]Department of Chemical and Petroleum Engineering, University of Pittsburgh, Pittsburgh, Pennsylvania 15261, USA
(Received 18 March 2014; published 25 September 2014)

We report *in situ* atomic-resolution transmission electron microscopy observations of the oxidation of stepped Cu surfaces. We find that the presence of surface steps both inhibits oxide film growth and leads to the oxide decomposition, thereby resulting in oscillatory oxide film growth. Using atomistic simulations, we show that the oscillatory oxide film growth is induced by oxygen adsorption on the lower terrace along the step edge, which destabilizes the oxide film formed on the upper terrace.

DOI: 10.1103/PhysRevLett.113.136104 PACS numbers: 68.37.Lp, 81.65.Mq, 82.45.Jn

The interaction of oxygen with metal surfaces has long attracted significant attention due to its technological importance. Nevertheless, many fundamental questions still remain unresolved, particularly concerning the early stages of oxidation. While models of oxygen surface adsorption have almost exclusively focused on terraces, a detailed understanding of the initial oxidation of surfaces has always been complicated by inhomogeneities caused by the presence of surface defects. Atomic steps—a defect common to crystal surfaces—are typically considered as active sites for both bond breaking and surface adsorption owing to the reduced coordination of atoms at step sites [1–3].

Here we describe dynamic, atomic-scale transmission electron microscopy (TEM) observations of the initial-stage oxidation of stepped Cu surfaces. Through the use of *in situ* TEM we are able to both spatially and temporally resolve oxide growth at the atomic scale. We observe that the presence of surface steps leads to decomposition of the oxide overlayer at the growth front, thereby resulting in oscillatory oxide growth that proceeds in tandem with the propagation of the surface step. Using density-functional theory (DFT) and *ab initio* molecular dynamics (AIMD), we show that the oxide decomposition at step edge is induced by O adsorption on the lower terrace that destabilizes the oxide film formed on the upper terrace.

The oxidation experiments were performed in a dedicated environmental TEM (FEI Titan 80-300) equipped with an objective-lens aberration corrector. Single-crystal Cu(100) films with ~500 Å thickness were grown on NaCl (100) by *e*-beam evaporation. The Cu films were subsequently removed from the substrate by dissolution of NaCl in deionized water, washed, and mounted on a TEM specimen holder. Any native Cu oxide was removed in the TEM by annealing the Cu film at ~400 °C in H_2 gas flow, which resulted in faceted holes in the Cu film. These Cu facets are oxide free and ideal for *in situ* TEM observations of oxidation. Within the range of temperature and pressure employed in the study, only Cu_2O is expected to form [4,5], which was also confirmed by *in situ* electron energy loss spectroscopy (EELS) analysis (see Supplemental Material [6]). The DFT calculations were performed using the Vienna *ab initio* simulation package (VASP) [7,8]. AIMD calculations were performed using VASP, starting from the DFT-relaxed structures (more details given in Supplemental Material [6]).

Figure 1(a) shows *in situ* high-resolution TEM images (captured from Movie S1) of a Cu(110) surface, seen edge-on at the oxygen pressure $pO_2 = 5 \times 10^{-3}$ Torr and T = 350 °C. The oxidation proceeds through the growth of a single Cu_2O layer on the Cu(110) surface [the oxide layer is about 4 Å thick, approximately three $Cu_2O(220)$ atomic layers]. The growth of the Cu_2O layer starts from the left corner and propagates along the surface. The Cu surface consists of two wide terraces separated by a step-bunched region ~5 Å in height, which corresponds to a high-index (430) facet (see Supplemental Material [6]). The *in situ* TEM observation shows that the oxide layer does not sweep across the stepped region unimpeded. Instead, the stepped region moves synchronously with the oxide growth. Such in-step propagation is interrupted when the substrate step flow does not keep up with the oxide growth, and the growth front of the oxide layer reaches the downward edge of the Cu terrace. The oxide layer is seen to retract from the terrace edge and then resumes its growth. Once the oxide growth front catches up with the step edge again, it undergoes another cycle of retraction and regrowth. Such oscillatory propagation occurs several times, until the stepped surface becomes completely flattened due to significant transport of Cu supplied from other surface regions in order to fill up the lower Cu terrace. The oxide overlayer then grows monotonically. Figure 1(b) shows the evolution in the length of

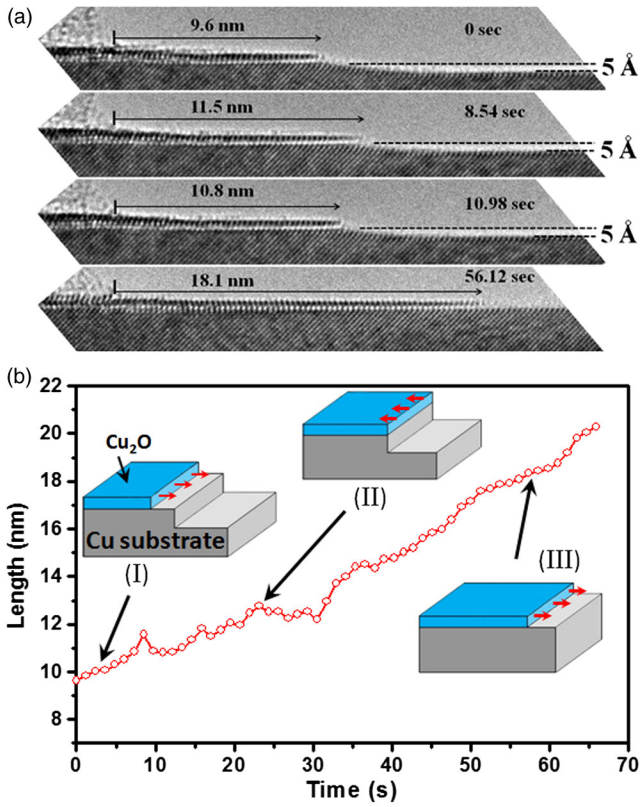

FIG. 1 (color online). (a) Sequence of high-resolution TEM images (Supplemental *in situ* TEM Movie S1 [6]) of a single Cu_2O layer on a stepped Cu(110) surface at 350 °C and $pO_2 = 5 \times 10^{-3}$. (b) Dependence of the growth length of the oxide film on time measured from the *in situ* TEM video [6]; insets show schematically the different growth stages of the oxide film with respect to the propagation of the surface step of the Cu substrate.

the oxide layer measured from the *in situ* TEM video [6]. Insets in Fig. 1(b) schematically show several key stages of the observed oscillation: (I) synchronous propagation of the oxide overlayer with the upper Cu terrace by step flow; (II) the oxide overlayer catches up with the downward edge of the Cu terrace when the oxide film grows faster than the step flow of the Cu terrace, resulting in retraction of the oxide layer; (III) monotonic oxide-film growth once the stepped substrate is flattened out.

Figure 2 presents *in situ* TEM images (Movie S2 [6]) of the oscillatory growth of a bilayer oxide film on a stepped Cu(110) surface (each oxide layer is about 4 Å thick). Figure 2(a) corresponds to the moment at which the growth front of the inner oxide layer reaches the descending edge of the Cu terrace while the growth front of the upper oxide layer is slightly behind that of the inner oxide layer. Figure 2(b) shows that the inner oxide layer retracts due to its proximity with the Cu terrace edge while the outer oxide layer continues to grow and catches up with the growth front of the inner oxide layer. As seen in Fig. 2(c), the inner oxide layer resumes its growth as the step-bunched region

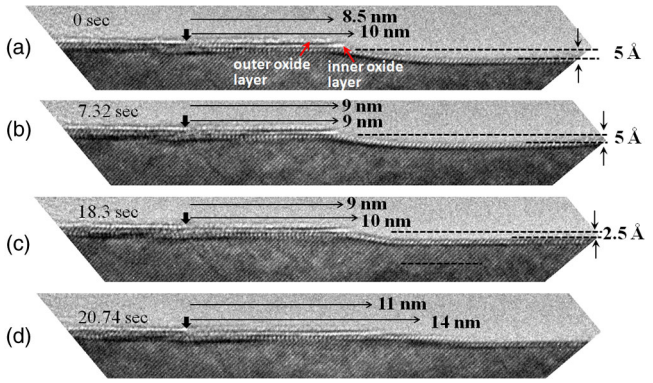

FIG. 2 (color online). *In situ* TEM observation of the growth of a bilayer oxide film on a stepped Cu(110) surface during the oxidation at 350 °C and $pO_2 = 5 \times 10^{-3}$ Torr (Supplemental *in situ* TEM Movie S2 [6]).

moves to the right. The bilayer oxide film does not sweep across the step-bunched region during the oxidation. Figure 2(d) shows that the oxide film grows monotonically once the stepped surface becomes flattened.

Figure 3 presents *in situ* TEM images (Movie S3 [6]) of the oxidation of a Cu(100) surface separated by a large step-bunched region (step height ~7 nm). The step-bunched region adjacent to the lower terrace evolves into a terrace with Cu adatoms detached from the step-bunched region. The oxide films nucleate at the step-edge corners and propagate to the left in tandem with the widening of the Cu terrace [Fig. 3(b)]. When the oxide layer grows faster than the rate at which the underlying Cu terrace widens, the oxide retracts at the downward edge of the Cu terrace [Fig. 3(c)]. The oxide layer restores its growth after the Cu terrace widens further [Fig. 3(d)]. Oxide formation on the upper-right terrace also occurs but does not sweep across the large step-bunched region, further revealing the pinning effect of surface steps on oxide growth. Figures 1–3 show that there is no (or very little) oxide formation on the planar surfaces (i.e., in which the normal is parallel to the electron beam), as inferred by the absence of moiré-fringe contrast in the TEM images [11]. One can also note that the TEM electron-beam irradiation has a negligible effect on the observed oscillatory oxide growth, as evidenced by the lack of oscillatory growth on flattened surface under the same *e*-beam irradiation condition.

The observations described above show that the surface-step-induced oscillatory oxide growth occurs for both Cu(100) and Cu(110), suggesting that the phenomenon is not tied to a particular step-edge configuration. Surface steps are known to play a significant role as effective trapping centers for O adsorption, preferentially passivating metal step-edge atoms rather than those on terraces [22–24]. The correlation between reactivity and properties of steps is, however, still an open question [2], while it is indeed the case that the oxide formation preferentially starts from step-terrace corners [25]. The *in situ* TEM observations

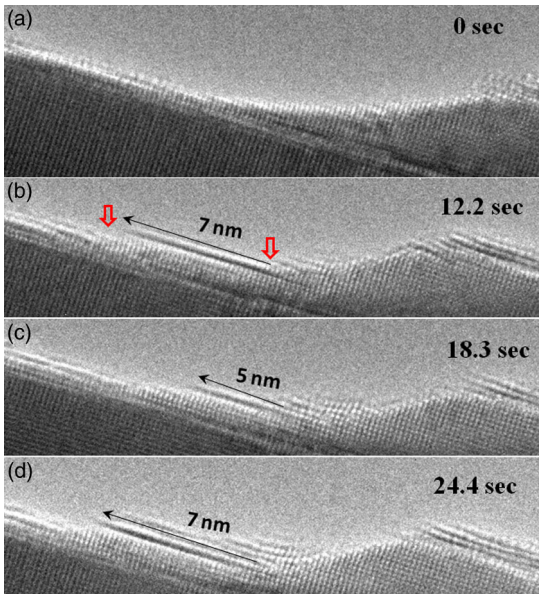

FIG. 3 (color online). *in situ* TEM images showing the nucleation and growth of a multiatomic-layer oxide film on Cu(100) terraces separated by a large step-bunched region at 350 °C and $pO_2 = 5 \times 10^{-3}$ Torr (Supplemental *in situ* TEM Movie S3 [6]). The oxide layers nucleate at the step-edge corners (indicated by red arrows) and grow laterally on the newly formed Cu terraces. They undergo retraction once they reach the terrace edge (the growth front of the oxide film formed on the lower-left terrace is drifting out of the field of the TEM view).

shown in Figs. 1–3 indicate that the oxide growth is inhibited by descendant steps that further cause oxide retraction from the step edge. This results in oscillatory oxide growth mediated by the step flow of the substrate. Surface steps can induce an additional diffusion barrier [i.e., Ehrlich-Schwoebel (ES) [26,27]] that hinders the descendent of adatoms to the lower terrace and thus favors three-dimensional growth [28–30]. However, the oxide films shown here grow two dimensionally via step flow, largely due to the elevated temperature that facilitates adatoms to overcome the ES barrier. Thus, the step-edge-induced oscillatory oxide growth is attributed to a thermodynamic origin rather than the kinetic effect of the ES barrier. We employ DFT calculations to examine various aspects of the oxidation process, including O adsorption as the oxide film approaches a terrace edge.

Modeling a system consisting of stepped (430) with a multiple-atomic-layer-thick oxide film as observed experimentally is far beyond current computational capability. However, because the (430) facet is composed of an alternate stacking of a three-atomic-spacing-wide (110) terrace and a monoatomic-height (100) step, we have chosen to model a stepped surface consisting of two (110) terraces separated by a single-atomic-wide (100) step, which forms a single unit of the (430) facet (see Supplemental Material [6]). We compute the system energy by growing a monolayer of Cu_2O on the upper terrace of a stepped Cu(110) surface. The initial oxidation of Cu(110) results in epitaxial $Cu_2O(110)$ film [31]. Cu_2O has a natural lattice misfit of 15.4% with the Cu substrate; this large misfit makes the formation of a coherent metal-oxide interface energetically unfavorable. The epitaxial growth of Cu_2O thin films on Cu substrates results in a (5×6) coincidence site lattice at the Cu_2O-Cu interface [11,32]. Using the (5×6) Cu_2O-Cu interface configuration, we calculate O adsorption energies as the oxide film approaches the step edge. As illustrated in Fig. 4(a), the oxide growth is simulated by sequentially adding Cu and O atoms onto the growth front of a preexisting oxide film on the Cu upper terrace. Figure 4(a) shows three representative equilibrium structures of the oxide-substrate system as more O and Cu atoms are added onto the oxide growth front, where the added O rows are numbered. Figure 4(b) shows the adsorption energy per O atom as a function of the added O rows, where row 4 corresponds to the descending edge of the upper terrace [Fig. 4(aiii)]. O adsorption energy decreases as more O is added, i.e., the oxide film becomes more stable as it approaches the terrace edge. Figure 4(aiii) shows that O atoms embed into the long-bridge sites between Cu atoms along the step edge. The increased coordination of O atoms with Cu at the step edge results in the enhanced stability of the oxide film.

Since the upper terrace is now fully covered by the oxide layer, we then consider further O adsorption at the lower terrace. We first find that the pseudothreefold positions are the most stable O adsorption sites as shown in the left image of Fig. 4(c). We employ AIMD simulations to elucidate the structural evolution of the oxide film with the O atoms adsorbed on the lower terrace. We start the dynamic simulation by heating the DFT-relaxed structure with two chemisorbed O atoms up to 700 K by velocity scaling, and then annealing at 700 K for 10 ps. The right image in Fig. 4(c) shows the final configuration after annealing, which shows that the step-edge region has experienced substantial distortion. Cu atoms at the terrace edge are dragged down by the adsorbed O with an average displacement of 0.95 Å from their original positions, while the two Cu atoms that are closely bonded with adsorbed O atoms show the most pronounced displacement of about 2.10 Å, which is close to the lattice spacing (2.57 Å) of Cu(110). The displacement of these step-edge Cu atoms results in vacant sites beneath the growth front of the oxide layer on the upper terrace. As a result, Cu atoms in the oxide layer (as denoted by Cu_O) diffuse down to the vacant site and the oxide film front becomes collapsed. As seen from the projection views of the two shaded areas [insets in Fig. 4(c)], O atoms 1 and 3 in the colinear O-Cu-O chain (left image) become next neighbors (right image) with the displacement of the Cu atom (denoted by 2), which may make the two O atoms unstable on the surface due to their repulsion force (note that simulations of O desorption associated with the oxide decomposition

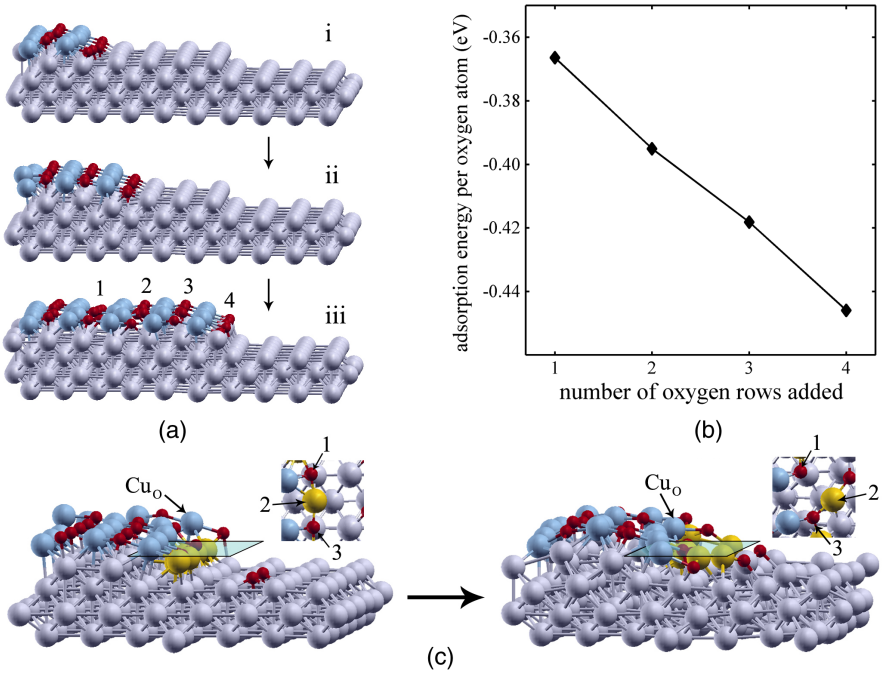

FIG. 4 (color online). (a) Minimum-energy structures for the monolayer Cu_2O growth on the upper terrace of a stepped Cu(110) surface by adding Cu and O atoms onto the oxide growth front as it approaches the terrace edge; (b) O adsorption energy as the oxide approaches the terrace edge; (c) minimum-energy structure of the system with an oxide layer on the upper terrace and chemisorbed O on the lower terrace (left), and the final snapshot of the system after being annealed at 700 K for 10 ps (right). Insets in (c) are projection views of the area of the shaded squares. O, red balls; Cu in the oxide layer, blue balls; Cu along the downward edge of the upper Cu terrace, yellow balls.

are computationally more challenging using AIMD). We have applied similar AIMD heating and annealing procedures with one and three O atoms adsorbed at the lower terrace (not shown): the results show the same trends of the morphology changes in the oxide film. It is also worth noting that the AIMD treatment on a system with no O atoms adsorbed at the lower terrace results in no obvious displacement of the step-edge Cu atoms.

The sequence of events shown in Fig. 4 corresponds to the most stable sites for oxygen adsorption identified from the DFT calculations. While O chemisorption can occur randomly, O adsorbed at unstable sites (e.g., terraces) does not lead to a stable oxide. This is in line with our *in situ* TEM observations that oxide growth occurs only at the growth front of an oxide film rather than randomly across the whole surface. Our DFT calculations using different step-edge configurations indicate that the conclusion described above does not depend on the specific step-edge configuration, suggesting that the gradual evolution of the stepped region does not change the oxide growth behavior. This is in line with our *in situ* TEM observations (Figs. 1–3), where the stepped facet evolves and can deviate from the (430) in the course of oxide growth.

The AIMD simulations reveal that O adsorption at the lower Cu terrace results in the shrinkage of approximately one lattice spacing (~2.6 Å) of the oxide layer from the step edge. However, as shown experimentally, the oxide layer may retract by up to 2 nm (see Fig. 3). AIMD simulation is thus not adequate to completely reproduce the continuous oxide retraction process, although there is a massive difference in time scales between the simulation and experiment here. We describe qualitatively why the oxide film can retract by such a large amount. By a close look at Figs. 3(b)–3(c), one can see that the Cu terrace also retracts during the oxide decomposition. This suggests that Cu atoms released from the oxide retraction are susceptible to detachment from the step edge; as a result, the oxide layer front is constantly within the proximity of the step edge. This process can be reversed only if the rate of the reattachment of Cu adatoms supplied from other surface regions to the terrace edge is faster than Cu detachment from the terrace edge. This allows for the upper Cu terrace to move ahead of the oxide-film growth front. As a result, the oxide film regains its growth without experiencing the destabilizing effect from O adsorption at the lower terrace. This is evident in Figs. 1 and 2, which show that the oxide film grows monotonically once the stepped Cu surface becomes flattened due to the fast lateral step flow of the Cu substrate.

In summary, we have observed the oscillatory interface motion during oxide growth on stepped Cu surfaces. Our *in situ* TEM observations show that the presence of surface steps pins the oxide film growth on the upper terrace and further destabilizes the oxide film, thereby resulting in the

observed oscillation. Our DFT and AIMD atomistic simulations demonstrate that the oxide instability is induced by O adsorption at the lower terrace along the step edge. This behavior does not depend on the step-edge configuration, implying the broader applicability of our results [33]. Oscillations in the rates of gas-surface reactions are observed in a wide range of systems [3,34–38]. Our results reveal the unique role of surface defects in oxidation and may have broader implications for understanding gas-surface reaction kinetics modulated by atomic defects on a solid surface.

This work was supported by the U.S. Department of Energy, Office of Basic Energy Sciences, Division of Materials Sciences and Engineering under Award No. DE-FG02-09ER46600. W. Saidi acknowledges the support of NSF under Grant No. DMR-1410055. Research was carried out in part at the Center for Functional Nanomaterials, Brookhaven National Laboratory, which is supported by the U.S. Department of Energy, Office of Basic Energy Sciences, under Contract No. DE-AC02-98CH10886, and at the National Center of Electron Microscopy, Lawrence Berkeley National Laboratory, which is supported by the U.S. Department of Energy, Office of Basic Energy Sciences, under Contract No. DE-AC02-05CH11231. This work used the Extreme Science and Engineering Discovery Environment (XSEDE), which is supported by National Science Foundation Grant No. OCI-1053575.

L. Li and L. Luo contributed equally to this work.

*To whom all correspondence should be addressed.
gzhou@binghamton.edu

[1] R. T. Vang, K. Honkala, S. Dahl, E. K. Vestergaard, J. Schnadt, E. Laegsgaard, B. S. Clausen, J. K. Nørskov, and F. Besenbacher, Nat. Mater. **4**, 160 (2005).
[2] L. Vattuone, L. Savio, and M. Rocca, Surf. Sci. Rep. **63**, 101 (2008).
[3] B. L. M. Hendriksen, M. D. Ackermann, R. van Rijn, D. Stoltz, I. Popa, O. Balmes, A. Resta, D. Wermeille, R. Felici, S. Ferrer, and J. W. M. Frenken, Nat. Chem. **2**, 730 (2010).
[4] X. Duan, O. Warschkow, A. Soon, B. Delley, and C. Stampfl, Phys. Rev. B **81**, 075430 (2010).
[5] W. A. Saidi, M. Lee, L. Li, G. Zhou, and A. J. H. McGaughey, Phys. Rev. B **86**, 245429 (2012).
[6] See Supplemental Material at http://link.aps.org/supplemental/10.1103/PhysRevLett.113.136104 for EELS analysis, detail of DFT calculation, and in situ TEM videos, which includes Refs. [7–21].
[7] G. Kresse and J. Hafner, Phys. Rev. B **49**, 14251 (1994).
[8] G. Kresse and J. Furthmüller, Comput. Mater. Sci. **6**, 15 (1996).
[9] J. P. Perdew, J. A. Chevary, S. H. Vosko, K. A. Jackson, M. R. Pederson, D. J. Singh, and C. Fiolhais, Phys. Rev. B **46**, 6671 (1992).
[10] G. Kresse and D. Joubert, Phys. Rev. B **59**, 1758 (1999).
[11] G. W. Zhou, L. L. Luo, L. Li, J. Ciston, E. A. Stach, and J. C. Yang, Phys. Rev. Lett. **109**, 235502 (2012).
[12] L. Li and G. W. Zhou, Surf. Sci. **615**, 57 (2013).
[13] M. Methfessel and A. T. Paxton, Phys. Rev. B **40**, 3616 (1989).
[14] H. J. Monkhorst and J. D. Pack, Phys. Rev. B **13**, 5188 (1976).
[15] N. W. Ashcroft and N. D. Mermin, *Solid State Physics* (Saunders College, Philadelphia, 1976).
[16] T. Kangas, K. Laasonen, A. Puisto, H. Pitkänen, and M. Alatalo, Surf. Sci. **584**, 62 (2005).
[17] M. Alatalo, S. Jaatinen, P. Salo, and K. Laasonen, Phys. Rev. B **70**, 245417 (2004).
[18] S. Y. Liem, G. Kresse, and J. H. R. Clarke, Surf. Sci. **415**, 194 (1998).
[19] S. Nosé, Mol. Phys. **52**, 255 (1984).
[20] P. Muller and A. Saul, Surf. Sci. Rep. **54**, 157 (2004).
[21] G. Prévot, Y. Girard, V. Repain, S. Rousset, A. Coati, Y. Garreau, J. Paul, N. Mammen, and S. Narasimhan, Phys. Rev. B **81**, 075415 (2010).
[22] J. G. Wang, W. X. Li, M. Borg, J. Gustafson, A. Mikkelsen, T. M. Pedersen, E. Lundgren, J. Weissenrieder, J. Klikovits, M. Schmid, B. Hammer, and J. N. Andersen, Phys. Rev. Lett. **95**, 256102 (2005).
[23] J. Gustafson, A. Resta, A. Mikkelsen, R. Westerström, J. N. Andersen, E. Lundgren, J. Weissenrieder, M. Schmid, P. Varga, N. Kasper, X. Torrelles, S. Ferrer, F. Mittendorfer, and G. Kresse, Phys. Rev. B **74**, 035401 (2006).
[24] M. Okada, L. Vattuone, M. Rocca, and Y. Teraoka, J. Chem. Phys. **136**, 094704 (2012).
[25] G. W. Zhou, L. L. Luo, L. Li, J. Ciston, E. A. Stach, W. Saidi, and J. C. Yang, Chem. Commun. (Cambridge) **49**, 10862 (2013).
[26] G. Ehrlich and F. G. Hudda, J. Chem. Phys. **44**, 1039 (1966).
[27] R. L. Schwoebel and E. J. Shipsey, J. Appl. Phys. **37**, 3682 (1966).
[28] R. Zhang and H. Huang, Appl. Phys. Lett. **98**, 221903 (2011).
[29] S. J. Liu, H. Huang, and C. H. Woo, Appl. Phys. Lett. **80**, 3295 (2002).
[30] M. G. Lagally and Z. Zhang, Nature (London) **417**, 907 (2002).
[31] G. W. Zhou and J. C. Yang, Appl. Surf. Sci. **222**, 357 (2004).
[32] G. W. Zhou, Appl. Phys. Lett. **94**, 233115 (2009).
[33] Similar oscillation in Al_2O_3 film growth in step-bunched regions on NiAl(100) was observed from our recent *in situ* low-energy electron microscopy observations of the initial oxidation of NiAl(100), which showed that the oxide growth results in significant step bunching of the NiAl substrate that, in turn, leads to oscillatory oxide growth (unpublished data).
[34] V. K. Medvedev, Y. Suchorski, and J. H. Block, Surf. Sci. **343**, 169 (1995).
[35] B. L. M. Hendriksen, S. C. Bobaru, and J. W. M. Frenken, Surf. Sci. **552**, 229 (2004).
[36] B. L. M. Hendriksen, S. C. Bobaru, and J. W. M. Frenken, Catal. Today **105**, 234 (2005).
[37] R. Imbihl and G. Ertl, Chem. Rev. **95**, 697 (1995).
[38] S. H. Oh, M. F. Chisholm, Y. Kauffmann, W. D. Kaplan, W. Luo, M. Rühle, and C. Scheu, Science **330**, 489 (2010).